Anisotropic constitutive modelling of rooted soils

ALI AKBAR KARIMZADEH*, ZHIWEI GAO† and ANTHONY KWAN LEUNG‡

The mechanical behaviour of rooted soils is anisotropic. In this work, an anisotropic constitutive model for rooted soils is developed, incorporating two independent fabric tensors to represent the soil fabric and the root network. The effect of root tensile strength mobilisation on soil's dilatancy and plastic hardening mechanism is addressed by introducing new fabric anisotropic variables (A_B, A_R), expressed as a joint invariant of fabric and loading direction tensors. A new root network evolution rule is proposed to capture the progressive root tensile strength mobilisation as the root orientation evolves towards the perpendicular direction of the major principal stress. The model is validated against test data. The model can predict the transition of sand's strain-softening to hardening upon undrained triaxial extension due to the presence of roots. The model predicts lower strength and more contraction for rooted silty sands than the bare case during drained triaxial compression, as the former has a higher void ratio due to root inclusion and minimal root tensile strength mobilisation (indicated by a high A_R and slow root network evolution rate). Conversely, during drained triaxial extension, the model exhibits higher shear strength and less contraction due to substantial root tensile strength mobilisation (indicated by a low A_R).

KEYWORDS: anisotropy; constitutive relations; fabric; stress path; structure of soils; vegetation

INTRODUCTION

Plants stabilise shallow soils by increasing the shear strength of the soil through the mobilisation of the roots' tensile strength owing to stress transfer along the soil–root interface (Stokes *et al*., 2014; Karimzadeh *et al*., 2024a). Recent studies have reported that the mechanical properties of rooted soils are anisotropic and stress-dependent upon monotonic (Muir Wood *et al*., 2016; Karimzadeh *et al*., 2021; Li *et al*., 2023; Karimzadeh *et al*., 2024a) and cyclic (Karimzadeh *et al*., 2021, 2022; Liu *et al*., 2024) loading conditions. The anisotropic behaviour of rooted soils in terms of failure criterion (Karimzadeh *et al*., 2024a), liquefaction resistance (Karimzadeh *et al*., 2021, 2022; Liu *et al*., 2024) and maximum shear modulus (Karimzadeh *et al*., 2024b) has been extensively investigated experimentally and theoretically. However, existing theories are not applicable for predicting soil deformation and stress–strain relationships in anisotropic rooted soils. Thus, developing an anisotropic constitutive model for rooted soils is essential to facilitate the analysis and design of vegetated infrastructure against their safety and serviceability.

In the literature, two approaches have been used to develop constitutive models for rooted soils. The first approach treats rooted soils as a continuum medium and develops models within the elastoplastic framework (Świtała & Wu, 2018; Świtała *et al*., 2019; Ng *et al*., 2024). Switala & Wu (2018) addressed the effects of roots on soil behaviour by introducing two parameters within a modified Cam Clay model to capture the effects of roots on hardening, considering strain-driven expansion of preconsolidation pressure. Similarly, Ng *et al*. (2024) proposed a state-dependent constitutive model for rooted soils in which the root-induced hardening phenomenon was modelled through the mechanisms of pore occupancy and bonding between soil particles due to plant roots' biochemical activities (Karimzadeh *et al*., 2024a). In the second approach, the soil and roots are deemed as separate phases that are governed by their constitutive model (Woodman *et al*., 2020; Meijer *et al*., 2023); therefore, the parameters and loading history of each phase need to be determined separately. The second approach provides a more in-depth understanding of the stress–strain relationship of each phase of a rooted soil than the first approach does. However, this modelling approach can be complicated and impractical because of the highly complex nature of the root architecture and characteristics (Woodman *et al*., 2020; Meijer *et al*., 2023). Meijer *et al*. (2023) developed a four-phase composite modelling technique to establish a constitutive framework for rooted soils. This model incorporated separate constitutive models for the root and soil phases, accounting for stress calculations in the root phase based on the principles of fibre reinforcement, considering gradual mobilisation of root tensile strength, rotations, root elongation and soil–root interfacial behaviour such as root slippage and breakage. Despite the success of these two modelling approaches, they are only valid or have only been validated against limited stress paths and cannot be used to predict the anisotropic behaviour of rooted soils under general three-dimensional (3D) loading conditions. Furthermore, no theory exists to address the anisotropy of rooted soils induced by roots and host soil simultaneously.

The behaviour of rooted soils is anisotropic because of two major factors, namely, the initial anisotropy resulting from the initial soil fabric and the root network

Manuscript received 5 July 2024; revised manuscript accepted 30 June 2025.

* Formerly Department of Civil and Environmental Engineering, Hong Kong University of Science and Technology, Hong Kong SAR, P. R. China; now Chair of Geotechnical Engineering and Institute of Geomechanics and Underground Technology, RWTH Aachen University, Aachen, Germany.
† Glasgow Computational Engineering Centre (GCEC), James Watt School of Engineering, University of Glasgow, Glasgow, UK.
‡ State Key Laboratory of Climate Resilience for Coastal Cities, Department of Civil and Environmental Engineering, Hong Kong University of Science and Technology, Hong Kong SAR, P. R. China (corresponding author: ceanthony@ust.hk).

(Karimzadeh *et al*., 2024a, 2024b). Meanwhile, both of them evolve during shearing (i.e. shear-induced anisotropy) (Li & Dafalias, 2002; Li *et al*., 2009; Golchin & Lashkari, 2014). As rooted soil is subjected to shearing, the orientation and arrangement of soil particles and roots continuously evolve (Meijer *et al*., 2023). Indeed, previous studies have demonstrated that straining a rooted soil progressively mobilises the roots' tensile strength, providing an increased contribution by the roots to the soil's shear strength, accompanied by the evolution of root orientation within the host soil (Karimzadeh *et al*., 2021, 2022; Meijer *et al*., 2023). Meijer *et al*. (2023) were among the first to propose a conceptual method to address the effect of root reorientation on the mobilisation of the root–soil interfacial friction. However, a theoretical explanation for how roots undergo reorientation during straining within the anisotropic critical state theory framework is lacking. In addition, no theory exists to capture the simultaneous evolution of the fabric of the host soil and the root network in a constitutive model and its contribution to mechanical behaviour.

In this study, the aim is to develop a constitutive model within the anisotropic critical state theory framework (ACST; Li & Dafalias, 2012) to capture the mechanical behaviour of rooted soils under general 3D loading conditions based on the well-established modelling frameworks previously developed by Li & Dafalias (2002) and Gao & Zhao (2015). Two independent fabric tensors that describe the internal structure of the host soil and the root are employed to address the effects of the soil fabric and root network on the anisotropic behaviour of rooted soil through the introduction of two anisotropic variables. These variables are expressed in terms of a joint invariant of the tensors about (*a*) the deviatoric loading direction, (*b*) the soil fabric and (*c*) the root network. A novel root network evolution rule is introduced to model the evolution of root orientation. Three additional parameters, compared with the original model for bare soil, are incorporated to describe the effects of roots on the mechanical behaviour of rooted soils. The model's performance is validated against existing datasets that comprehensively reported the stress path effects on rooted soils of different overconsolidation ratios (OCRs) under drained and undrained conditions.

MODEL FRAMEWORK

The anisotropic constitutive model for rooted soils is developed based on the frameworks proposed by Li & Dafalias (2002). The ACST (Li & Dafalias, 2012) is employed to incorporate the influences of (*a*) fabric anisotropy and its evolution, (*b*) the root network and (*c*) the evolution of the root orientation on the mechanical behaviour of rooted soils. The basic model framework is introduced here, and more details of the key model formulations will be given in the next section, including the fabric tensors, plastic modulus and dilatancy.

The cone-shaped yield surface is used in this model (Li & Dafalias, 2002)

$$f(r_{ij}, H) = \frac{R}{g(\theta)} - H = 0 \tag{1}$$

$$R = \sqrt{\frac{3}{2} r_{ij} r_{ij}} \tag{2}$$

where R is the second stress ratio invariant, which provides a general definition of 3D deviatoric stress ratios; r_{ij} is the stress ratio tensor equal to s_{ij}/p; s_{ij} is the deviatoric stress tensor equal to $\sigma_{ij} - p\delta_{ij}$; σ_{ij} is the stress tensor; p is the mean effective stress; δ_{ij} is the Kronecker delta (=1 for $i = j$; and 0 otherwise); H is the size of the yield surface; and the interpolation function $g(\theta)$ represents the relationship between the critical state stress ratio and the Lode angle θ as follows (Li & Dafalias, 2002):

$$g(\theta) = \frac{\sqrt{(1+c^2)^2 + 4c(1-c^2)\sin 3\theta} - (1+c^2)}{2(1-c)\sin 3\theta} \tag{3}$$

where $c = M_e/M_c$, with M_c and M_e being the values of the critical stress ratios at triaxial compression and triaxial extension, respectively. The critical state stress ratio for rooted soils is assumed to be the same as that of bare soils (Karimzadeh *et al*., 2021). The Lode angle (θ) is equal to $\theta = -1/3 \sin^{-1}\left(3\sqrt{3}/2 \times J_{3D}/J_{2D}^{3/2}\right)$ where $J_{3D} = 1/3\ s_{ij}\ s_{jk}\ s_{ki}$ and $J_{2D} = 1/2\ s_{mn}\ s_{mn}$.

The condition of consistency of the yield function is expressed as (Li, 2002; Gao & Zhao, 2015)

$$\mathrm{d}f = p n_{ij} \mathrm{d}r_{ij} - \langle \mathrm{d}L \rangle K_p \tag{4}$$

where

$$n_{ij} = \frac{\dfrac{\partial f}{\partial r_{ij}} - \dfrac{1}{3}\left(\dfrac{\partial f}{\partial r_{mn}}\right)\delta_{mn}\delta_{ij}}{\left\| \dfrac{\partial f}{\partial r_{ij}} - \dfrac{1}{3}\left(\dfrac{\partial f}{\partial r_{mn}}\right)\delta_{mn}\delta_{ij} \right\|}$$

and K_p is the plastic modulus (defined later). The condition of consistency can also be written in other forms, as explained in Li (2002) and Gao & Zhao (2015). The plastic strain increment $\mathrm{d}\varepsilon_{ij}^p$ of the model is expressed as

$$\mathrm{d}e_{ij}^p = \langle \mathrm{d}L \rangle n_{ij} \tag{5}$$

$$\mathrm{d}\varepsilon_v^p = D\sqrt{\frac{2}{3}\mathrm{d}e_{ij}^p \mathrm{d}e_{ij}^p} = \sqrt{\frac{2}{3}}\langle \mathrm{d}L \rangle D \tag{6}$$

$$\mathrm{d}\varepsilon_{ij}^p = \mathrm{d}e_{ij}^p + \frac{1}{3}\mathrm{d}\varepsilon_v^p \delta_{ij} = \langle \mathrm{d}L \rangle \left(n_{ij} + \sqrt{\frac{2}{27}} D \delta_{ij} \right) = \langle \mathrm{d}L \rangle N_{ij} \tag{7}$$

where $\mathrm{d}\varepsilon_v^p$ is the plastic volumetric strain increment; $\mathrm{d}e_{ij}^p$ is the plastic deviatoric strain increment; D is the dilatancy relationship; $\mathrm{d}L$ is the loading index; and $\langle \square \rangle$ are the Macauley brackets rendering $\langle \mathrm{d}L \rangle = \mathrm{d}L$ for $\mathrm{d}L > 0$ and $\langle \mathrm{d}L \rangle = 0$ for $\mathrm{d}L \leq 0$.

The elastic stress–strain relationship can be expressed as

$$\mathrm{d}e_{ij}^e = \frac{\mathrm{d}s_{ij}}{2G} = \frac{p\mathrm{d}r_{ij}}{2G} + \frac{r_{ij}\mathrm{d}p}{2G} \tag{8}$$

$$\mathrm{d}\varepsilon_v^e = \frac{\mathrm{d}p}{K} \tag{9}$$

where G is the elastic shear modulus and K is the elastic bulk modulus. Both G and K are assumed to be independent of root inclusion. The elastic shear modulus proposed by Richart *et al*. (1970) is used in the model

$$G = G_0 \frac{(2 \cdot 97 - e)^2}{1+e}\sqrt{p p_a} \tag{10}$$

where G_0 is a model parameter; p_a is the atmospheric pressure (=101 kPa) and e is the void ratio. In calculating the void ratio of rooted soil, roots are considered as part of the solid phase. The elastic bulk modulus is a function of G and Poisson's ratio v as follows:

$$K = G\frac{2(1+v)}{3(1-2v)} \tag{11}$$

Indeed, fabric anisotropy and root networks could influence the soil's elastic properties (Lashkari, 2010, 2016;

Zhao & Gao, 2016; Karimzadeh *et al.*, 2024a), but this feature was not considered in the model due to the lack of experimental data about the elastic properties of rooted soils and for the simplicity of modelling.

DERIVATION OF THE CONSTITUTIVE EQUATIONS

Multiplying equation (8) by n_{ij} on both sides and using the condition of consistency (equation (4)) and the relations $n_{ij}\delta_{ij} = n_{ii} = 0$ and $n_{ij}n_{ij} = 1$ yields

$$2Gn_{ij}\mathrm{d}e^{\mathrm{e}}_{ij} = pn_{ij}\mathrm{d}r_{ij} + n_{ij}r_{ij}\mathrm{d}p = \mathrm{d}LK_{\mathrm{p}} + n_{ij}r_{ij}\mathrm{d}p \tag{12}$$

Incorporating equations (5) and (9) into equation (12) and the relations $n_{ij}\mathrm{d}e_{ij} = n_{ij}\mathrm{d}\varepsilon_{ij}$ and $\mathrm{d}\varepsilon_{\mathrm{v}} = \delta_{ij}\mathrm{d}\varepsilon_{ij}$ returns

$$2Gn_{ij}\left(\mathrm{d}\varepsilon_{ij} - \frac{1}{3}\mathrm{d}\varepsilon_{\mathrm{v}}\delta_{ij} - \mathrm{d}Ln_{ij}\right) = \mathrm{d}LK_{\mathrm{p}} + n_{ij}r_{ij}K\left(\mathrm{d}\varepsilon_{mn}\delta_{mn} - D\sqrt{\frac{2}{3}}\mathrm{d}L\right) \tag{13}$$

Given that $2Gn_{ij}\delta_{ij} = 0$, the expression for $\mathrm{d}L$ can be determined based on equation (13)

$$\langle \mathrm{d}L\rangle = \frac{2Gn_{kl} - Kn_{nm}r_{nm}\delta_{kl}}{K_p + 2G - \sqrt{2/3}Kn_{pq}r_{pq}D}d\varepsilon_{kl} = \Pi_{kl}d\varepsilon_{kl} \tag{14}$$

where Π_{kl} is self-evident.

The stress increment can be expressed in terms of E_{ijkl}, as follows:

$$\mathrm{d}\sigma_{ij} = E_{ijkl}(\mathrm{d}\varepsilon_{kl} - \langle \mathrm{d}L\rangle N_{kl}) \tag{15}$$

where E_{ijkl} is the elastic strain, which is defined as

$$E_{ijkl} = (K - 2G)\delta_{ij}\delta_{kl} + 2G\delta_{ik}\delta_{jl} \tag{16}$$

The complete stress–strain relationship of the model can be obtained by combining equations (14) and (15)

$$\mathrm{d}\sigma_{ij} = [E_{ijkl} - h(\mathrm{d}L)E_{ijmn}N_{mn}\Pi_{kl}]\,\mathrm{d}\varepsilon_{kl} = \Lambda_{ijkl}\,\mathrm{d}\varepsilon_{kl} \tag{17}$$

where Λ_{ijkl} is the elastoplastic tensor, and $h(\mathrm{d}L)$ is the Heaviside step function, with $h(\mathrm{d}L > 0) = 1$ and $h(\mathrm{d}L < 0) = 1$.

FABRIC TENSORS AND ANISOTROPIC VARIABLES

Fabric tensors are needed to model the anisotropic mechanical behaviour of soils (Li & Dafalias, 2002, 2012; Gao *et al.*, 2014; Lu *et al.*, 2019). In the proposed model, two fabric tensors are employed – one for the bare soil (F_{ij}) and the other for the root network in the soil ($\mathcal{R}_{ij}$). The definition of F_{ij} can be found in previous studies (Li & Dafalias, 2012; Gao *et al.*, 2014). For a transversely isotropic soil considering the isotropic plane in the x–y plane, the initial F_{ij} is expressed as

$$F_{ij} = \begin{bmatrix} F_{zz} & 0 & 0 \\ 0 & F_{xx} & 0 \\ 0 & 0 & F_{yy} \end{bmatrix} = \sqrt{\frac{2}{3}}\begin{bmatrix} F_0 & 0 & 0 \\ 0 & \dfrac{-F_0}{2} & 0 \\ 0 & 0 & \dfrac{-F_0}{2} \end{bmatrix} \tag{18}$$

where $|F_0|$ is the initial degree of anisotropy of the fabric of bare soils. As a first approximation, the root network in soils is also considered transversely anisotropic (Karimzadeh *et al.*, 2024a); hence, $\mathcal{R}_{ij}$ can be expressed as follows when the x–y plane is the isotropic plane:

$$\mathcal{R}_{ij} = \begin{bmatrix} \mathcal{R}_{zz} & 0 & 0 \\ 0 & \mathcal{R}_{xx} & 0 \\ 0 & 0 & \mathcal{R}_{yy} \end{bmatrix} = \sqrt{\frac{2}{3}}\begin{bmatrix} \mathcal{R}_0 & 0 & 0 \\ 0 & -\dfrac{\mathcal{R}_0}{2} & 0 \\ 0 & 0 & -\dfrac{\mathcal{R}_0}{2} \end{bmatrix} \tag{19}$$

where $|R_0|$ is the initial degree of anisotropy of the root network.

Existing studies have shown that the soil fabric evolves with plastic deformation, gradually aligning with the direction of the deviatoric loading (Li & Dafalias, 2012; Zhao & Guo, 2015). Following this phenomenon, the fabric evolution law in the proposed model can be expressed as

$$\mathrm{d}F_{ij} = \langle \mathrm{d}L\rangle k_{\mathrm{f}}(n_{ij} - F_{ij}) \tag{20}$$

where k_{f} is the rate of fabric evolution (Li & Dafalias, 2012; Gao *et al.*, 2014). The fabric tensor in equation (20) was assumed to be stress independent. To improve the accuracy of the prediction of the peak shear strength and the K_0 consolidation behaviour, the incorporation of a stress ratio-dependent fabric tensor (Seyedi Hosseininia, 2013; Lashkari *et al.*, 2019; Norouzi & Lashkari, 2021; Liao *et al.*, 2022; Mugele *et al.*, 2024) for the case of rooted soils should be explored in the future.

Existing experimental evidence has demonstrated that the root network in soil evolves with plastic deformation (Meijer *et al.*, 2023). Numerous existing studies have demonstrated progressive utilisation of roots' tensile properties upon straining, causing substantial increases in the shear strength of rooted soils (Karimzadeh *et al.*, 2021, 2024a; Meijer *et al.*, 2023). This phenomenon means that the root network evolves to maximise the roots' mobilised tensile stress to resist shearing (i.e. more roots evolve towards the direction of tensile strain in the soils; Fig. 1). Following this phenomenon, the evolution of $\mathcal{R}_{ij}$ is proposed as

$$\mathrm{d}\mathcal{R}_{ij} = \langle \mathrm{d}L\rangle k_{\mathrm{r}}(-n_{ij} - \mathcal{R}_{ij}) \tag{21}$$

where k_{r} is the rate of root network evolution. The formulation means that the direction of the root network evolves and aligns perpendicularly to the direction of the deviatoric loading. This alignment is modelled when the eigenvectors associated with the major and minor eigenvalues of the n_{ij} tensor are swapped with each other, resulting in the $-n_{ij}$ tensor. Under this condition, the root network approaches a perpendicular alignment with the direction of the major principal stress. As a result, the majority of the root network will align with the direction of the soil's tensile strain, mobilising most of the root tensile strength in the root network. For example, during triaxial compression, the root network evolves to align with the radial direction, where the maximum tensile strain occurs in a vegetated soil sample (Karimzadeh *et al.*, 2024a).

Two fabric anisotropic variables (FAVs) A_{B} and A_{R} are defined in the model (Li & Dafalias, 2012) to describe the effect of the anisotropy in bare soil and roots on soil behaviour (Karimzadeh *et al.*, 2024a), as follows:

$$A_{\mathrm{B}} = F_{ij}n_{ij} \tag{22a}$$

$$A_{\mathrm{R}} = \mathcal{R}_{ij}n_{ij} \tag{22b}$$

The FAVs are incorporated into the dilatancy state parameter ζ, following Li & Dafalias (2012) as follows:

$$\zeta = \psi - e_{\mathrm{A}}(A_{\mathrm{B}} - 1) + e_{\mathrm{R}}(A_{\mathrm{R}} - 1) \tag{23}$$

where e_{A} and e_{R} are two model parameters, where e_{R} is associated with the location of the critical state in the

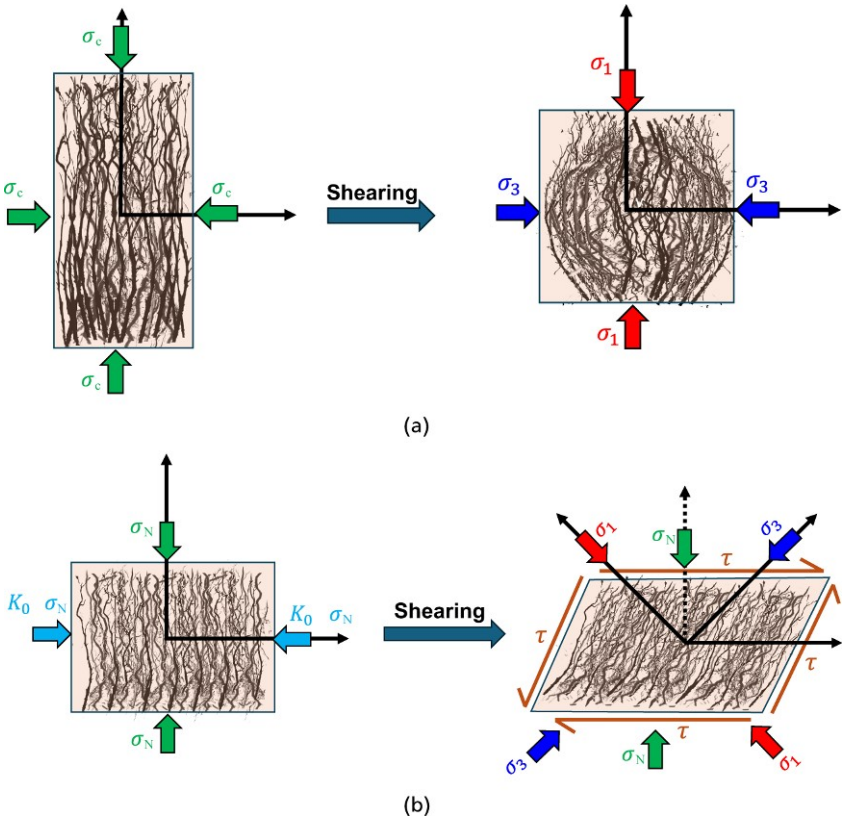

Fig. 1. Root reorientation upon (a) triaxial compression path and (b) simple shear stress path. σ_1 is the major principal stress; σ_3 is the minor principal stress; σ_N is the normal stress; τ is the shear stress; and K_0 is the coefficient of earth pressure at rest

e–log(p') space. Accordingly, e_R is dependent on the root volume ratio (RVR, representing the root content by volume). $\psi = e - e_c$ is the state parameter defined by Been & Jefferies (1985); and e_c is the critical state void ratio of the host soil for the current p and e. The critical state line (CSL) for sand (Li & Wang, 1998; equation (24a)) and silty sand (Chiu & Ng, 2003; equation (24b)) can be expressed as follows:

$$e_c = e_\Gamma - \lambda_c \left(\frac{p}{p_a}\right)^{\xi} \tag{24a}$$

$$e_c = e_\Gamma - \lambda_c \log(p) \tag{24b}$$

where e_Γ, λ_c and ξ are model parameters. The new dilatancy state variable (ζ), in equation (23), was introduced to address the effect of root tensile mobilisation on soil behaviour. This variable depends on the loading direction relative to the root network (that is A_R) and is incorporated into the constitutive equations, such as the plastic modulus and dilatancy (see further details later). Specifically, a smaller A_R value – indicating a loading direction closer to perpendicular to the root network and hence a smaller ζ based on equation (23) – means greater exposure of the root network to the soil's tensile strain and greater mobilisation of the root tensile strength. Previous studies have demonstrated that tensile mobilisation increases when the direction of the reinforcement elements become more perpendicular to that of the major principal stress (Diambra & Ibraim, 2015; Muir Wood *et al.*, 2016; Gao & Diambra, 2021; Karimzadeh *et al.*, 2024a).

The critical state behaviour of rooted soil has not been thoroughly studied yet. Thus, the influence of roots on the location of the CSL in e–p space remains uncertain. Nevertheless, the effect of roots on the location of CSL in the e–p space cannot be ignored because roots occupy voids in the soil and affect the soil dilatancy (Karimzadeh *et al.*, 2021), thereby affecting the value of the critical state void ratio. At the critical state, rooted soil is assumed always to have a higher void ratio than bare soil for any given p (Fig. 2). This assumption has been reflected in equation (23), which states that the location of the CSL of rooted soils is above that of the bare soil because $A_R = -1$ and $e_R(A_R - 1) = -2e_R$ at the critical state condition (Fig. 2).

PLASTIC MODULUS AND DILATANCY RELATIONSHIP

The plastic modulus of rooted soils in the proposed model can be expressed as follows (Gao & Zhao, 2015):

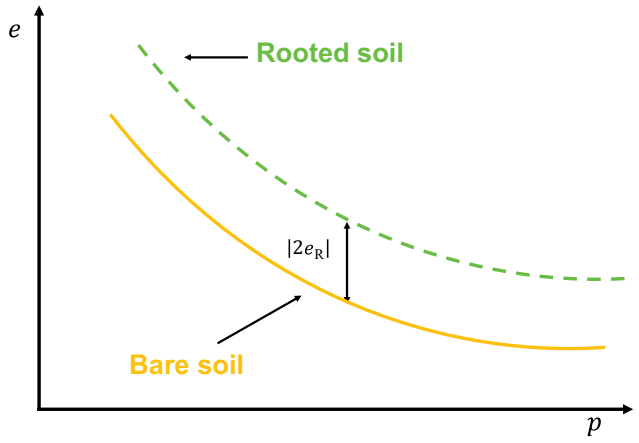

Fig. 2. Illustration of the effect of roots on the location of the critical state lines (CSLs) in the in e–p space, where e is the void ratio and p is the mean effective stress. e_R is a model parameter that controls the location of the CSL of rooted soil in e–p space

$$K_p = \frac{Gh}{R}\left[M_c g(\theta)\exp(-n\zeta) - R\right] \quad (25)$$

$$h = (1 - h_1 e)\exp(h_2 A_B) \quad (26)$$

where n is a model parameter and h is a factor for the plastic modulus to be dependent upon e and A_B, as proposed by Gao & Zhao (2015). The dilatancy equation equates external and internal work rates, with internal work expressed as a function of the dilatancy state variable (ζ), intrinsic critical state parameters and the invariants of the stress tensor (Li & Dafalias, 2002, 2012; Gao *et al.*, 2014). The internal work depends directly on the loading direction with respect to the root network tensor (i.e. A_R), linking dilatancy to the rate of root tensile mobilisation. The dilatancy relationship of rooted soils can be expressed as follows:

$$D = \frac{d_0}{M_c g(\theta)}\left(1 + \frac{R}{M_c g(\theta)}\right)\left[M_c g(\theta)\exp(m\zeta) - R\right] \quad (27)$$

where m and d_0 are positive model parameters. Varying the dilatancy state variable ζ in equation (23), which depends on the root network, can capture the effects of roots on plastic hardening and dilatancy of the soil.

DATASETS USED FOR MODEL VALIDATION

Two datasets are selected for model evaluation, namely, (*a*) the undrained triaxial compression and extension tests of saturated artificial rooted sand (Karimzadeh *et al.*, 2021; Table 1); and (*b*) the drained triaxial compression and extension tests of saturated normal consolidated (NC) and overconsolidated (OC) cultivated rooted silty sand (Karimzadeh *et al.*, 2024a; Table 2). In the first dataset, Toyoura sand ($e_{max} = 0{\cdot}977$, $e_{min} = 0{\cdot}597$, $D_{50} = 0{\cdot}22$ mm) was dry pluviated over a network of vetiver roots (*Chrysopogon zizanioides* L.) that were distributed predominantly vertically to form triaxial samples.

The relative density of the samples was 64%. The RVR (ratio of the volume of roots to the total sample volume) was 0·64%. Undrained triaxial compression and extension tests were conducted on these artificial rooted samples at effective confinements of 15, 30, 100 and 200 kPa (Table 1). In the second dataset, multiple triaxial silty sand samples were statically compacted to the same dry density of 1488 kg/m^3 and cultivated with vetiver grass. After growing for 12–15 months and producing vegetated samples with RVR varying from 0·26 to 0·71%, they were subjected to drained triaxial compression and extension again at mean effective stresses of 50, 100 and 150 kPa (Karimzadeh *et al.*, 2024a). Notably, the roots in the samples were treated as solid phase when determining the void ratio of rooted soils.

MODEL VALIDATION

The proposed model has 18 parameters in total, and they can be categorised into five groups: (*a*) group 1, elasticity (G_0 and υ); (*b*) group 2, critical state (M_c, c, e_Γ, λ_c and ξ); (*c*) group 3, dilatancy (d_0 and m); (*d*) group 4, hardening (h_1, h_2 and n); and (*e*) group 5, fabric evolution (F_0, R_0, e_A, e_R, k_f and k_R) . Among the 18 parameters, three of them are used to model the effects of roots (namely, R_0, e_R and k_r). For group 1, G_0 and υ can be determined by measuring the maximum shear modulus of bare soil at the very small strain range (Karimzadeh *et al.*, 2024b) by fitting with equation (10) (Li & Dafalias, 2000). For group 2, all the critical state parameters can be obtained by determining the critical stress ratios upon compression and extension (M_c, c) and the CSL in the e–p plane (e_Γ, λ_c and ξ) of bare soil. A limited study (Karimzadeh *et al.*, 2021) has shown that the presence of roots did not affect M_c and c substantially; hence, the same values of M_c and c applied to the rooted soils. The remaining parameters were determined by best-fitting the deviatoric stress–deviatoric strain, stress path in the p–q plane and volumetric strain–deviatoric strain curves of the bare and rooted soils (e.g. Li & Dafalias, 2012; Gao & Zhao, 2013). Alternatively, one can use the automatic parameter determination methods developed by Rahman *et al.* (2005) to optimise the parameters. In particular, to calibrate the parameters R_0, k_r and e_R, that capture root effects, the parameter R_0 is typically set to be approximately 0·7, reflecting the predominant vertical growth pattern of tap rooted species. Ideally, the parameter e_R, which is a function of the RVR of soil, can be calibrated using the location of the CSL of rooted soil expressed in e–log(p') space for a given RVR. However, determining the location of the CSL in rooted soils can be challenging, because the samples often reach this state at rather large strains (i.e. approximately 100%; Fig. 3). Such a large strain range is normally not attainable in conventional triaxial apparatus, but might be possible for simple

Table 1. Summary of undrained triaxial tests on the artificial bare and rooted samples upon compression and extension reported in Karimzadeh *et al.* (2021)

Test	Sample type	RVR: %	Test condition	p_{in}: kPa	e_c
CB15	Bare	0	Undrained triaxial compression	15	0·733
CR15	Rooted	0·45		15	0·741
CB30	Bare	0		30	0·732
CR30	Rooted	0·45		30	0·740
CB100	Bare	0		100	0·725
CR100	Rooted	0·45		100	0·732
CB200	Bare	0		200	0·719
CR200	Rooted	0·45		200	0·727
EB15	Bare	0	Undrained triaxial extension	15	0·733
ER15	Rooted	0·45		15	0·741
EB30	Bare	0		30	0·732
ER30	Rooted	0·45		30	0·739
EB100	Bare	0		100	0·726
ER100	Rooted	0·45		100	0·733
EB200	Bare	0		200	0·718
ER200	Rooted	0·45		200	0·729

Note: RVR is the root volume ratio; p_{in} is the effective confining pressure; e is the void ratio of the sand–root composite after consolidation

Table 2. Summary of drained triaxial tests on normal consolidated (NC) and overconsolidated (OC) (overconsolidation ratio, OCR = 3) bare and cultivated samples upon compression and extension reported in Karimzadeh *et al.* (2024a)

Test ID	Type of sample	p_{in}: kPa	OCR	RVR: %	Void ratio		Stress path
					Initial	Consolidation	
					e_i	e_c	
Normal consolidated samples							
CB50	Bare	50	1	0	0·757	0·727	Compression
CB100		100	1	0	0·757	0·641	
CB150		150	1	0	0·757	0·630	
EB50	Bare	50	1	0	0·757	0·694	Extension
EB100		100	1	0	0·757	0·651	
EB150		150	1	0	0·757	0·618	
CR50	Rooted	50	1	0·57	0·740	0·712	Compression
CR100		100	1	0·61	0·738	0·657	
CR150		150	1	0·67	0·736	0·631	
ER50	Rooted	50	1	0·68	0·736	0·707	Extension
ER100		100	1	0·30	0·747	0·673	
ER150		150	1	0·37	0·746	0·640	
Overconsolidated samples							
CB50	Bare	50	3	0	0·757	0·610	Compression
CB100		100	3	0	0·757	0·529	
CB150		150	3	0	0·757	0·492	
EB50	Bare	50	3	0	0·757	0·616	Extension
EB100		100	3	0	0·757	0·544	
EB150		150	3	0	0·757	0·522	
CR50	Rooted	50	3	0·45	0·743	0·626	Compression
CR100		100	3	0·26	0·749	0·573	
CR150		150	3	0·71	0·735	0·555	
ER50	Rooted	50	3	0·39	0·745	0·649	Extension
ER100		100	3	0·52	0·762	0·549	
ER150		150	3	0·33	0·747	0·577	

Note: p_{in} is the effective confining pressure; OCR is the overconsolidation ratio; RVR is the root volume ratio; e_i is the initial void ratio before consolidation; e_c is the void ratio after consolidation

shear or ring shear apparatus. An alternative calibration approach for k_r and e_R involves the following procedures: the plastic hardening modulus (K_p, equation (25)) must become zero at the peak shear strength during drained triaxial compression and extension tests. To achieve this, these two parameters can be iteratively adjusted until K_p reaches zero at the peak state. Because the evolution of the root network tensor is influenced by k_r and e_R, this calibration process requires multiple iterations to complete the calibration. The values of R_0, k_r and e_R can be determined through trial and error, should the drained test data be unavailable. Tables 3 and 4 summarise the parameters that were used in this model for the artificial and cultivated rooted soil samples, respectively. For the former case, the critical state parameters for the Toyoura sand were taken from Li & Dafalias (2000). It is important to note that e_A and e_R need to be calibrated separately: e_A was first calibrated using the bare soil's data, and then e_R was independently calibrated using the rooted soil's data.

After the calibration of the model parameters, the F_0 value of the artificial rooted samples that were prepared by the dry deposition method was 0·7. In contrast, the cultivated samples that were prepared by static compaction under moist conditions returned an F_0 value of −0·1. The parameter F_0, which ranges from $-\frac{1}{\sqrt{6}}$ (indicating fabric alignment predominantly in the vertical direction with negligible horizontal fabric) to $\sqrt{\frac{2}{3}}$ (indicating fabric alignment predominantly in the horizontal direction with negligible vertical fabric), was calibrated by comparing the model predictions with the results of triaxial extension and compression tests conducted at the same p' of 100 kPa. After calibration, the F_0 value for the artificially rooted samples prepared by the dry deposition method was 0·7. This number suggests a remarkable difference in soil behaviour between the compression and extension stress path, with greater strength observed under compression. In contrast, cultivated samples prepared by the static compaction under moist conditions yielded an F_0 value of −0·1, suggesting more isotropic behaviour of the soil and reduced differences in the soil behaviour under compression and extension conditions. The difference in the values of F_0 indicates that during dry deposition, soil particles in the artificial samples tended to align more horizontally along their elongation, whereas the fabric of the cultivated samples was more isotropic when prepared under the moist condition. Indeed, the findings reported by scanning electron microscopy (SEM) analysis of samples (e.g. Ni *et al.*, 2021) and 3D X-ray computed tomography of the samples with different sample preparations (Shi *et al.*, 2021) have demonstrated that the distribution of particle orientation under moist conditions tended to be isotropic, indicating no clear preferential particle orientation due to the constraints imposed by matric suction.

In both the artificial and cultivated samples, the R_0 value is about 0·7, suggesting that the majority of roots orientated vertically. In the proposed model, k_f and k_r control the evolution rate of soil fabric and root network due to straining, respectively. The k_f value of the artificial samples made of Toyoura sand was substantially lower than that of the cultivated samples made of silty sand; the large difference implies that, compared with the sand, the fabric evolution occurred at a faster rate in the silty sand, in which the particles aligned more rapidly towards the direction of the

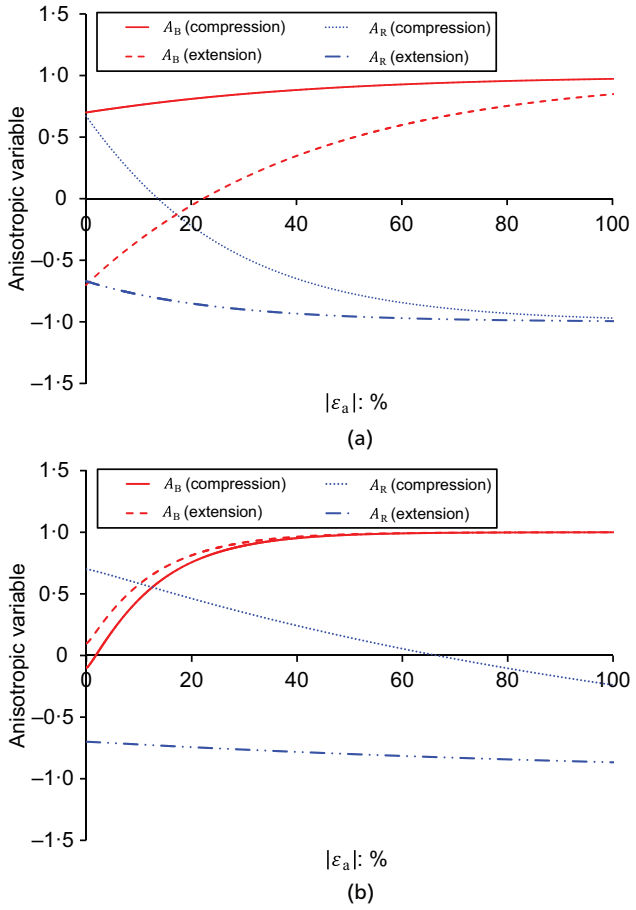

Fig. 3. Model prediction of the two anisotropic variables, A_B and A_R, varying with absolute axial strain ($|\varepsilon_a|$) under compression and extension stress paths: (a) artificial rooted samples under undrained condition; (b) cultivated rooted sample under drained condition

Table 3. Summary of the model parameters used for the artificial rooted sand samples

Elasticity	Critical state	Dilatancy	Hardening	Fabric evolution
$G_0 = 125$ $\nu = 0{\cdot}15$	$M_c = 1{\cdot}25$ $c = 0{\cdot}75$ $e_\Gamma = 0{\cdot}934$ $\lambda_c = 0{\cdot}019$ $\xi = 0{\cdot}7$	$d_0 = 0{\cdot}25$ $m = 1{\cdot}5$	$h_1 = 1$ $h_2 = 0{\cdot}9$ $n = 1$	$F_0 = 0{\cdot}7$ $R_0 = 0{\cdot}67$ $e_A = 0{\cdot}085$ $e_R = 0{\cdot}090$ $k_f = 3$ $k_r = 5$

Table 4. Summary of the model parameters used for the cultivated rooted silty sand samples

Elasticity	Critical state	Dilatancy	Hardening	Fabric evolution
$G_0 = 125$ $\nu = 0{\cdot}15$	$M_c = 1{\cdot}40$ $c = 0{\cdot}9$ $e_\Gamma = 0{\cdot}935$ $\lambda_c = 0{\cdot}086$ $\xi = \text{NA}$	$d_0 = 0{\cdot}5$ $m = 5$	$h_1 = 0{\cdot}9$ $h_2 = 0{\cdot}95$ $n = 0{\cdot}5$	$F_0 = -0{\cdot}1$ $R_0 = 0{\cdot}7$ $e_A = 0{\cdot}085$ $e_R = 0{\cdot}040$ $k_f = 10$ $k_r = 1$

deviatoric loading. The faster rate of fabric evolution can be attributed to the presence of more fine contents in the silty sand samples, which facilitated smoother particle rolling upon shearing (Fu & Dafalias, 2011). The k_r value of the artificial samples was larger than that of the cultivated samples, implying more substantial evolution of the root network in the former. This difference might arise from the rougher texture of the soil particles in sandy soil. Furthermore, the tests conducted on artificial samples were performed under undrained conditions, resulting in a significant increase in confining pressure due to soil dilatancy. This substantial increase in confining pressure inhibits roots from sliding against the soil (Gao & Zhao, 2013), thus allowing the root network to evolve more rapidly (hence a greater k_r value) than the case of cultivated samples tested under a drained condition.

The predicted fabric evolution is shown first to facilitate the discussion of model prediction of the stress–strain relationship below. The predicted variations of A_B and A_R with absolute axial strain $|\varepsilon_a|$ are shown in Fig. 3. As $|\varepsilon_a|$ increases, A_B increases and A_R reduces monotonically towards their respective critical value, at which both fabrics do not evolve further based on the ACST (Li & Dafalias, 2012). In the artificial samples, A_B reached the critical value at a $|\varepsilon_a|$ upon compression (60%) compared with the extension case (100%). However, for the cultivated samples, A_B reached the critical value upon both compression and extension paths at a similarly low $|\varepsilon_a|$ of 30%. The differences in the behaviour between the host soil in the artificial and cultivated samples occur because the latter has a more isotropic fabric, and the fabric evolution mainly involves the change in magnitude, enabling the evolutions of the soil fabric to reach their respective critical values at a similar rate in triaxial compression and extension. In both the artificial and cultivated samples, A_R reached the respective critical value at a lower value of $|\varepsilon_a|$ upon triaxial extension than upon triaxial compression. This phenomenon can be attributed to the closer alignment of the direction of the root network perpendicular to that of the deviatoric loading during extension, because the roots are predominantly vertically distributed in both the artificial and cultivated samples and are thus mostly perpendicular to the direction of the major principal stress upon extension. Overall, the model is capable of correctly simulating the evolution of the soil fabric and root network following both the triaxial compression and extension paths within the ACST framework.

The model's unique feature to capture the evolution is the reason for the success in the prediction of anisotropic behaviour of rooted soils. Effects of RVR (i.e. a measure of root content, by volume) can be considered in the model by relating e_R in equation (23) with RVR. Should the dataset about the effects of RVR on the behaviour of rooted soils be available, further work is needed to derive a relationship between e_R and RVR.

MODEL PREDICTION OF ROOTED SOIL RESPONSE

Artificial rooted Toyoura sand

Figure 4 shows the model prediction of bare sand in undrained triaxial compression and extension with different confining pressures. Upon compression (Fig. 4), the bare sample displayed a strain-hardening behaviour (increase in q with axial strain), followed a transitional strain-softening (decrease in q with axial strain) or quasi-state condition (constant q as axial strain increases) accompanied by a remarkable strain-hardening upon extension. The stress paths (Figs 4(c) and 4(d)) show that the sample exhibited a more contractive behaviour upon the extension compared with compression at the same confining pressure, which is attributable to the anisotropy of the soil fabric (Fig. 3).

Figure 5 shows the model prediction for tests on rooted sand in triaxial compression and extension. Evidently, the

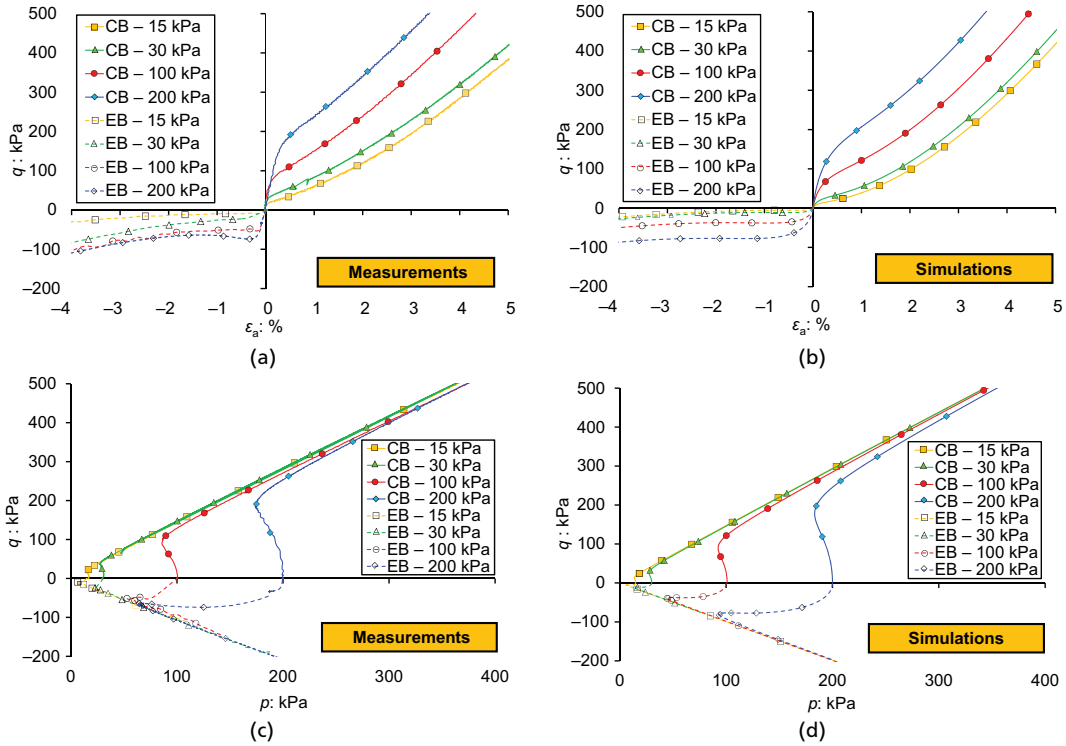

Fig. 4. Comparison of measurements and simulations of (a), (b) q–ε_a curves and (c), (d) stress paths of bare sand samples subjected to undrained compression and extension. CB and EB denote compression in bare sample and extension in bare sample, respectively

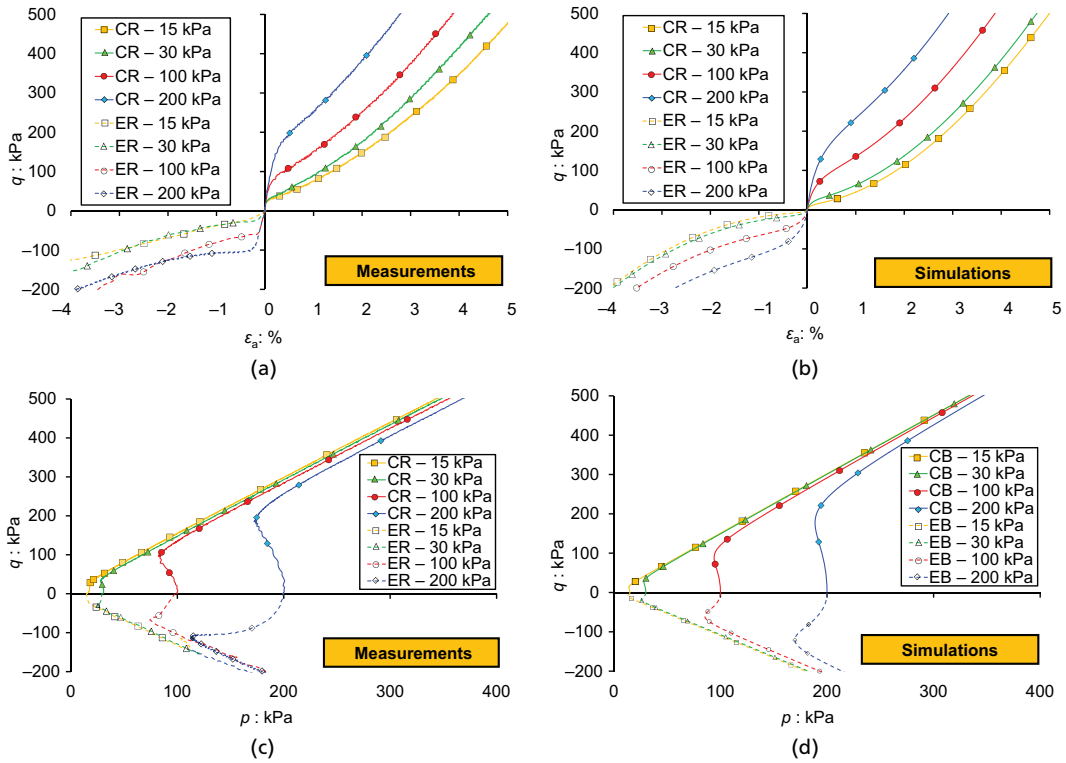

Fig. 5. Comparison of measurements and simulations of (a), (b) q–ε_a curves and (c), (d) stress paths of artificial rooted sand samples subjected to undrained compression and extension. CR and ER denote that the rooted sample was subjected to compression and extension, respectively

roots do not have a significant influence on soil response in triaxial compression because the value of A_R is high, which indicates less mobilisation of root strength and a minimal effect of the presence of roots on the dilatancy of soil, according to equation (23). In triaxial extension, rooted soil shows much higher shear strength (higher q at the same axial strain) and more dilative response (higher p at the same q in the effective stress path) than the bare soil because A_R is close to its critical value (i.e. critical value is equal to −1) at the strain range of lower than 5% (Fig. 3).

Importantly, the strain-softening behaviour observed in the bare sample upon extension switched to strain-hardening in the rooted samples; such a phenomenon can be well captured by the model, highlighting the necessity to have considered both soil anisotropy and the root network in the constitutive equations. Because of the missing data regarding the undrained and drained behaviour of loose rooted sands in the literature, evaluation of the proposed model against this kind of test condition should be performed, should more data become available in the future.

Cultivated silty sand samples under NC and OC conditions

Figures 6 and 7 show the comparison between model predictions and test data on NC silty sand. In triaxial compression, the peak shear strength of the rooted samples, at any confining pressure, is always lower than that of the bare samples, as illustrated in both measurements (Figs 6(a) and 7(a)) and simulations (Figs 6(b) and 7(b)).

This phenomenon is attributed to two reasons. First, the void ratios of the rooted samples are higher than those of the bare samples (Table 2). As a result, the rooted samples were less compressible than the bare counterpart because the roots that occupied some voids of the host soil resisted isotropic confinements (Karimzadeh *et al.*, 2024b). Second, during triaxial compression, the roots' tensile strength has limited mobilisation because most roots are initially parallel to the major principal stress (or direction of compression). Significant mobilisation of root tensile strength can only be achieved at a very large strain ($\varepsilon_a > 30\%$), which is beyond the peak strength state. This phenomenon can be seen from the evolution of A_R in Fig. 3.

In triaxial extension, due to the substantial mobilisation of root tensile strength because most roots orient along the minor principal stress direction (or direction of tension; A_R in Fig. 3), the peak shear strength of the rooted samples is always higher than that of the bare soil at all of the confining pressures considered. Similarly, the model can effectively capture such behaviour, despite the higher void ratio in the rooted samples compared with the bare soil, by introducing A_R in the dilatancy state parameter and plastic modulus of the soil.

In terms of dilatancy, generally speaking, the model is able to capture the increase in the volumetric contraction in triaxial compression or the decrease in the volumetric contraction in triaxial extension due to the presence of roots. However, some noticeable discrepancies between the measured and simulated volumetric responses, especially in triaxial extension, can be identified (Figs 6(c) and 6(d) and Figs 7(c) and 7(d)). These discrepancies may be attributed to experimental error in the determination of the actual void ratio, which is known to be sufficiently sensitive to affect the soil's volume change substantially (Diambra *et al.*, 2010). This practical difficulty is especially true for the case of rooted soils because measuring their void ratio is less straightforward compared with the bare case. In addition, the occurrence of strain localisation and non-uniform deformation of the rooted samples, especially in triaxial extension, might contribute to the discrepancies (Lade, 2002).

Figures 8 and 9 show the model prediction of OC bare and rooted silty sand. Although the model can largely capture the effects of confining pressure, stress paths and the effects of roots on the soil behaviour, it underestimates the initial stiffness and shear strength and did not capture the dilatancy behaviour. This discrepancy arises from the model's yield function. With this yield function, previous consolidation history affects the void ratio, which influences the soil stiffness, strength and dilatancy.

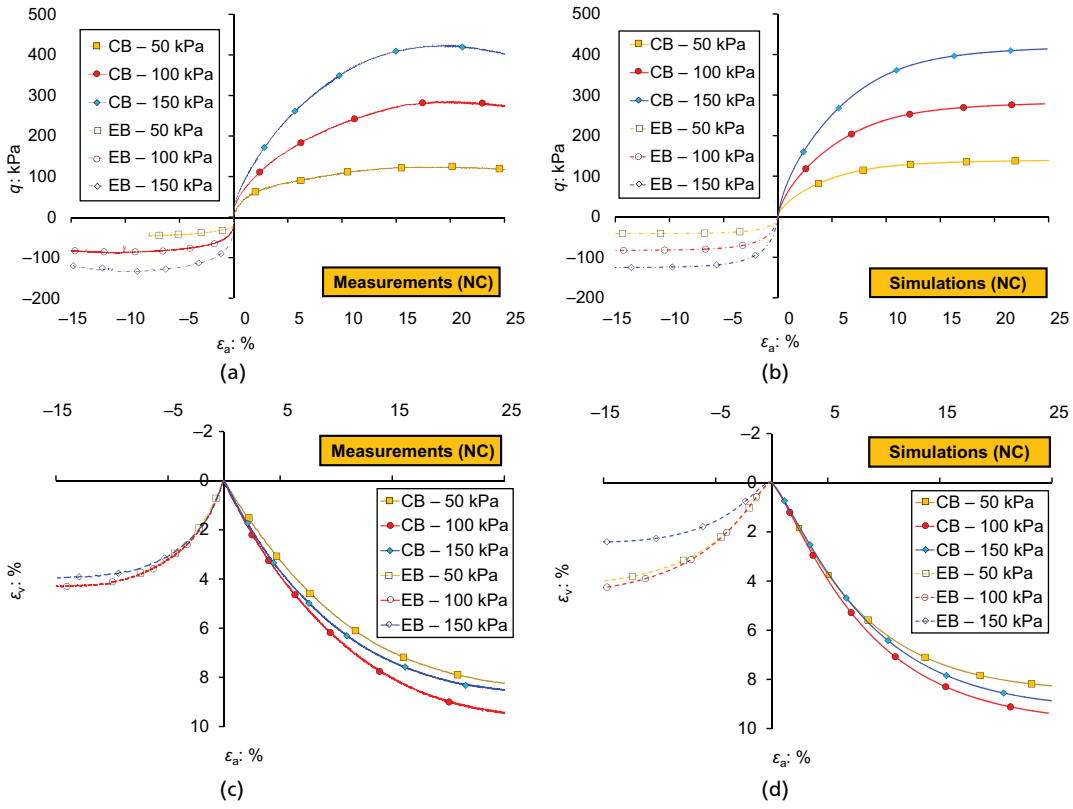

Fig. 6. Comparison of measurements and simulations of (a), (b) q–ε_a curves and (c), (d) $-\varepsilon_v$–ε_a curves of normal consolidated (NC) bare silty sand samples subjected to drained compression and extension. CB and EB denote that the bare sample was subjected to compression and extension, respectively

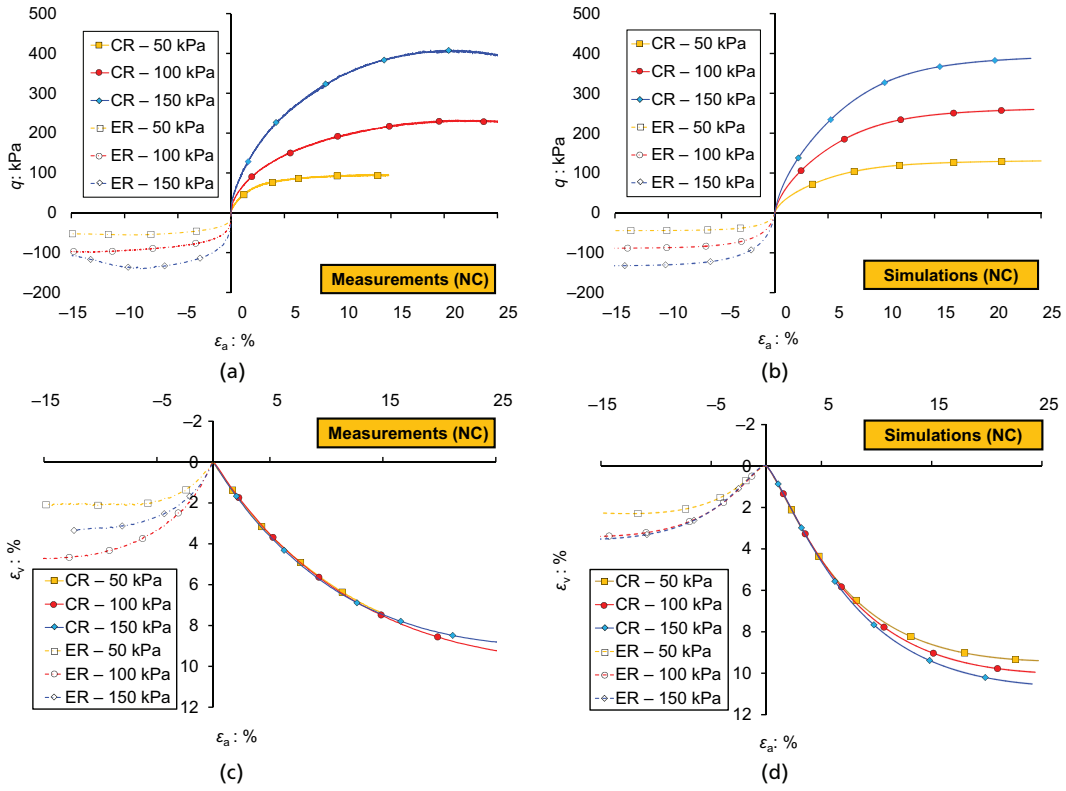

Fig. 7. Comparison of measurements and simulations of (a), (b) q–ε_a curves and (c), (d) $-\varepsilon_v$–ε_a curves of NC rooted silty sand samples subjected to drained compression and extension. CR and ER indicate that the rooted sample was subjected to compression and extension, respectively

However, overconsolidation can also cause other changes in the soil's internal structure, which affects the stress–strain relationship. It is worth noting that the effect of overconsolidation on the behaviour of silty sand tested under a drained condition could be different from those under an undrained condition (e.g. Lashkari *et al.*, 2022). Including a cap for the yield surface is expected to give a better prediction of overconsolidated soil behaviour under the undrained condition.

CONCLUDING REMARKS

An anisotropic multiaxial constitutive model has been developed for rooted soils within the ACST framework. The anisotropic behaviour of soil due to the internal structure of the host soil and the root system is captured by incorporating two new anisotropic variables, namely, A_B and A_R, into the dilatancy state parameter, ζ. These anisotropic variables are expressed as joint invariants of the deviatoric loading direction tensor (n_{ij}), deviatoric soil fabric (F_{ij}) and the root network fabric ($\mathcal{R}_{ij}$) tensors.

A new and unique feature of the proposed model is its capability to correctly capture the evolution of the fabric of the host soil and root network upon plastic straining. The root network evolution law drives the root orientation to move towards the direction of tension in the soil. Such evolution enables the progressive mobilisation of root tensile strength, which has an influence on soil stiffness, shear strength and dilatancy.

The proposed model has been validated by existing datasets of rooted soils tested under different drainage conditions, stress paths and initial void ratios. The model provides good predictions for bare and rooted sand in triaxial compression and extension with different confining pressures. An increased root reinforcement effect is observed in triaxial extension because more roots are initially perpendicular to the major principal stress direction. In triaxial compression, however, the root reinforcement effect is minimal as significant plastic strain is needed to mobilise the tensile strength of roots. For silty sand, the model can give a reasonable prediction when the soil is normally consolidated. However, the model does not predict the dilatancy of OC silty sand well with and without roots. This phenomenon could be due to the yield surface employed in this model, which predicts elastic response when the soil is subjected to overconsolidation. Better model prediction could be achieved if a bounding surface with a cap is used.

This paper represents the first step towards constitutive modelling of rooted soils. More work in future can be conducted to improve the model in several aspects. (*a*) The root fabric tensor is used to describe the root orientation in soils; its initial degree of anisotropy is assumed as a model parameter that has to be determined using the triaxial test data. A possible approach may be to use in situ X-ray computed tomography to gain a more comprehensive understanding of how the root network affects the soil fabric and its evolution during shearing. (*b*) The model assumes that the CSL location in the e–p plane is affected by root inclusion for simplicity, yet only little research is available in this regard. Discrete-element modelling might be used to study the critical state of rooted soil as large deformation can be applied without causing strain localisation. (*c*) The model can be implemented in any finite-element code for analysing practical boundary value problems. Depending on the root depth (i.e. either from field measurements or estimation through, for instance, root–soil ratio), a root zone of a given thickness can be defined, and the model can be specified in this zone to model the mechanical behaviour of root-reinforced soils. (*d*) This model should be further developed to

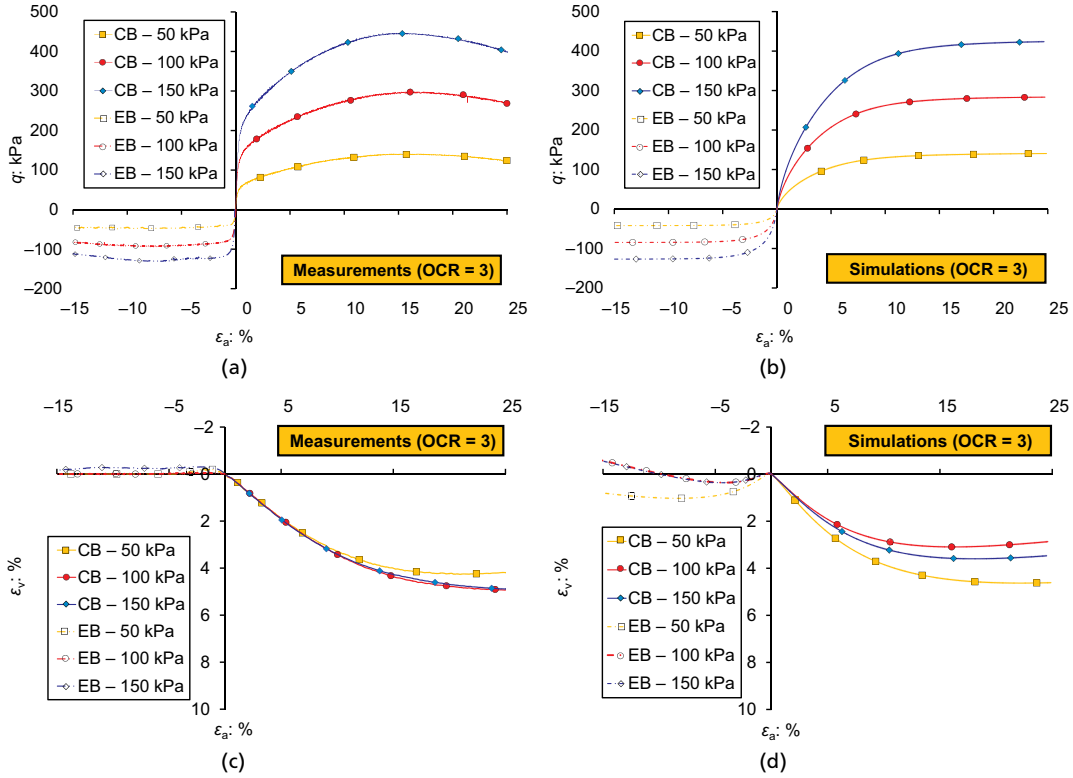

Fig. 8. Comparison of measurements and simulations of (a), (b) q–ε_a curves and (c), (d) $-\varepsilon_v$–ε_a curves of overconsolidated (OC) bare silty sand samples (overconsolidation ratio, OCR = 3) subjected to drained compression and extension. CB and EB denote that the bare sample was subjected to compression and extension, respectively

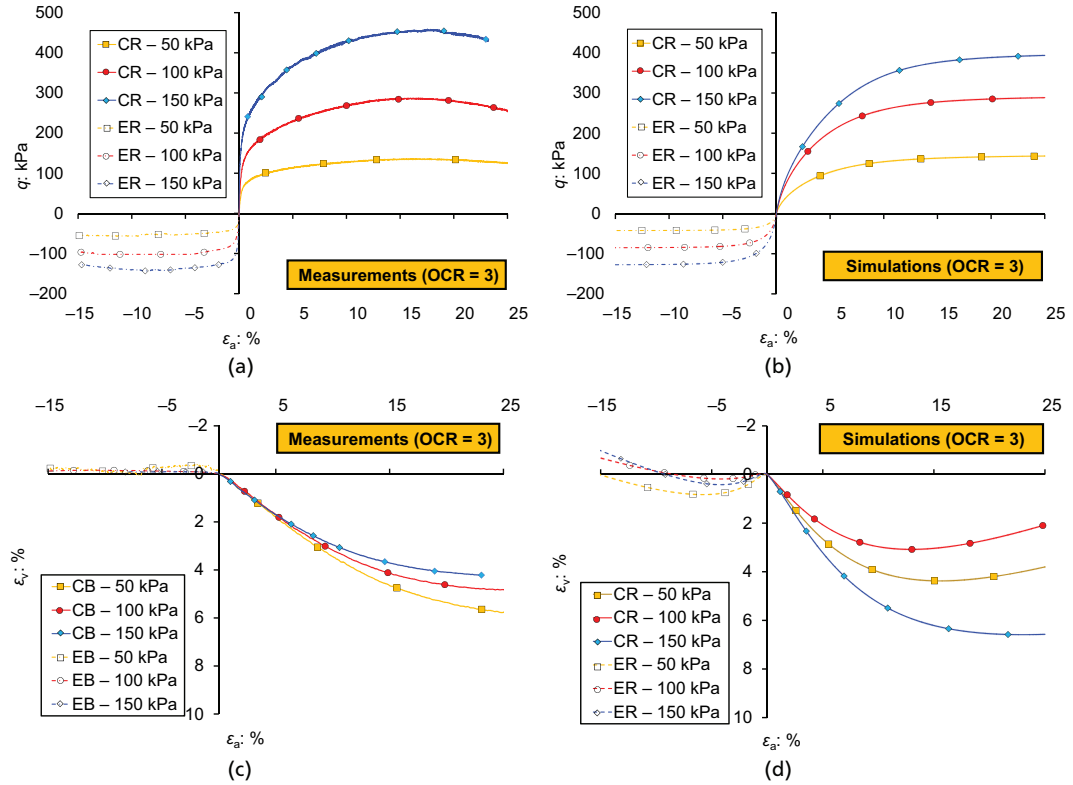

Fig. 9. Comparison of measurements and simulations of (a), (b) q–ε_a curves and (c), (d) $-\varepsilon_v$–ε_a curves of OC rooted silty sand samples (OCR = 3) subjected to drained compression and extension. CR and ER denote that the rooted sample was subjected to compression and extension, respectively

incorporate the effect of roots on the elastic properties of soil, which was neglected in the current study. Moreover, more experiments should be conducted on rooted soils with a wider range of root volume, so that its influence on the root-induced changes in soil fabric can be more accurately captured and evaluated.

FUNDING

The first and third authors acknowledge the financial support provided by the General Research Fund (grant no. 16207521, N_HKUST/603/22) funded by the Hong Kong Research Grants Council and also the grant ITC-SKLCRCC26EG01. The second author would like to acknowledge the support of the International Exchanges 2022 Cost Share (NSFC) fund provided by the Royal Society (grant no. IEC\NSFC\223020).

NOTATION

A_B	fabric anisotropic variables for soil fabric
A_R	fabric anisotropic variables for root network
D	dilatancy equation
d_0	model parameter
$\mathrm{d}L$	loading index
e	void ratio
e_A, e_R and e_Γ	model parameters
e^e_{ij} and e^p_{ij}	elastic and plastic deviatoric strain
F_{ij}	deviatoric soil fabric tensor
F_0	degree of soil fabric anisotropy
f	yield function
G	elastic shear modulus
G_0	model parameter
$g(\theta)$	interpolation function for the critical state stress ratio
h_1 and h_2	model parameters
K	elastic bulk modulus
M_c, M_e	critical state stress ratio in triaxial compression and triaxial extension
m	model parameter
p	mean stress
p_a	atmospheric pressure
R	stress ratio
$\mathcal{R}_{ij}$	deviatoric root network tensor
R_0	degree of root network anisotropy
r_{ij}	stress ratio tensor
s_{ij}	deviatoric stress tensor
δ_{ij}	Kronecker delta
ε_{ij}	total strain tensor
ζ	dilatancy state parameter
θ	Lode angle of the stress tensor
λ_c	model parameter
ν	Poisson's ratio
ξ	model parameter
σ_{ij}	stress tensor
ψ	state parameter for bare soil

REFERENCES

Been, K. & Jefferies, M. G. (1985). A state parameter for sands. *Géotechnique* **35**, No. 2, 99–112, 10.1680/geot.1986.36.1.123.

Chiu, C. F. & Ng, C. W. W. (2003). A state-dependent elasto-plastic model for saturated and unsaturated soils. *Géotechnique* **53**, No. 9, 809–829, 10.1680/geot.2003.53.9.809.

Diambra, A. & Ibraim, E. (2015). Fibre-reinforced sand: Interaction at the fibre and grain scale. *Géotechnique* **65**, No. 4, 296–308, 10.1680/geot.14.P.206.

Diambra, A., Ibraim, E., Muir Wood, D. & Russell, A. R. (2010). Fibre reinforced sands: Experiments and modelling. *Geotext. Geomembr.* **28**, No. 3, 238–250, 10.1016/j.geotexmem.2009.09.010.

Fu, P. & Dafalias, Y. F. (2011). Fabric evolution within shear bands of granular materials and its relation to critical state theory. *Numer. Analyt. Methods Geomech.* **35**, No. 18, 1918–1948, 10.1002/nag.988.

Gao, Z. & Diambra, A. (2021). A multiaxial constitutive model for fibre-reinforced sand. *Géotechnique* **71**, No. 6, 548–560, 10.1680/jgeot.19.P.250.

Gao, Z. & Zhao, J. (2013). Evaluation on failure of fiber-reinforced sand. *J. Geotech. Geoenviron. Engng* **139**, No. 1, 95–106, 10.1061/(ASCE)GT.1943-5606.0000737.

Gao, Z. & Zhao, J. (2015). Constitutive modeling of anisotropic sand behavior in monotonic and cyclic loading. *J. Engng Mech.* **141**, No. 8, e04015017, 10.1061/(asce)em.1943-7889.0000907.

Gao, Z., Zhao, J., Li, X. S. & Dafalias, Y. F. (2014). A critical state sand plasticity model accounting for fabric evolution. *Int. J. Numer. Analyt. Methods Geomech.***38**, No. 4, 370–390, 10.1002/nag.2211.

Golchin, A. & Lashkari, A. (2014). A critical state sand model with elastic–plastic coupling. *Int. J. Solids Structs* **51**, No. 15–16, 2807–2825.

Karimzadeh, A. A., Kwan Leung, A. & Amini, P. F. (2022). Energy-based assessment of liquefaction resistance of rooted soil. *J. Geotech. Geoenviron. Engng* **148**, No. 1, 1–5, 10.1061/(asce)gt.1943-5606.0002717.

Karimzadeh, A. A., Leung, A. K. & Gao, Z. (2024a). Shear strength anisotropy of rooted soils. *Géotechnique* **74**, No. 10, 1033–1046, 10.1680/jgeot.22.00103.

Karimzadeh, A. A., Leung, A. K. & Gao, Z. (2024b). Maximum shear modulus anisotropy of rooted soils. *Géotechnique*, 10.1680/jgeot.23.00496 (in press).

Karimzadeh, A. A., Leung, A. K., Hosseinpour, S., Wu, Z. & Fardad Amini, P. (2021). Monotonic and cyclic behaviour of root-reinforced sand. *Can. Geotech. J.* **58**, No. 12, 1915–1927, 10.1139/cgj-2020-0626.

Lade, P. V. (2002). Instability, shear banding, and failure in granular materials. *Int. J. Solids Structs* **39**, No. 13–14, 3337–3357, 10.1016/S0020-7683(02)00157-9.

Lashkari, A. (2010). A SANISAND model with anisotropic elasticity. *Soil Dyn. Earthq. Engng* **30**, No. 12, 1462–1477, 10.1016/j.soildyn.2010.06.015.

Lashkari, A. (2016). Prediction of flow liquefaction instability of clean and silty sands. *Acta Geotech.* **11**, No. 5, 987–1014, 10.1007/s11440-015-0413-9.

Lashkari, A., Khodadadi, M., Binesh, S. M. & Rahman, M. M. (2019). Instability of particulate assemblies under constant shear drained stress path: DEM approach. *Int. J. Geomech.* **19**, No. 6, e04019049, 10.1061/(ASCE)GM.1943-5622.0001407.

Lashkari, A., Shourijeh, P. T., Khorasani, S. S. S., Irani, N. & Rahman, M. M. (2022). Effects of over-consolidation history on flow instability of clean and silty sands. *Acta Geotech.* **17**, No. 11, 4989–5007, 10.1007/s11440-022-01502-y.

Li, S., Wang, Z. & Stutz, H. H. (2023). State-of-the-art review on plant-based solutions for soil improvement. *Biogeotechnics* **1**, No. 3, 100035, 10.1016/j.bgtech.2023.100035.

Li, X. S. (2002). A sand model with state-dependent dilatancy. *Géotechnique* **52**, No. 3, 173–186, 10.1680/geot.2002.52.3.173.

Li, X. S. & Dafalias, Y. F. (2000). Dilatancy for cohesionless soils. *Géotechnique* **50**, No. 4, 449–460.

Li, X. S. & Dafalias, Y. F. (2002). Constitutive modeling of inherently anisotropic sand behavior. *J. Geotech. Geoenviron. Engng* **128**, No. 10, 868–880, 10.1061/(asce)1090-0241(2002)128:10(868).

Li, X. S. & Dafalias, Y. F. (2012). Anisotropic critical state theory: Role of fabric. *J. Engng Mech.* **138**, No. 3, 263–275, 10.1061/(asce)em.1943-7889.0000324.

Li, X. S. & Wang, Y. (1998). Linear representation of steady-state line for sand. *J. Geotech. Geoenviron. Engng* **124**, No. 12, 1215–1217, 10.1061/(ASCE)1090-0241(1998)124:12(1215).

Li, X., Yu, H. S. & Li, X. S. (2009). Macro–micro relations in granular mechanics. *Int. J. Solids Structd* **46**, No. 25–26, 4331–4341, 10.1016/j.ijsolstr.2009.08.018.

Liao, D., Yang, Z., Wang, S. & Wu, W. (2022). Hypoplastic model with fabric change effect and semifluidized state for post-liquefaction cyclic behavior of sand. *Numer. Analyt. Methods Geomech.* **46**, No. 17, 3154–3177, 10.1002/nag.3444.

Liu, S., Li, J., Lyu, S., Fang, Y., Ji, X. & Ni, J. (2024). Deformation characteristics of root-reinforced soil under traffic induced cyclic loading. *Transp. Geotech.* **49**, 101424.

Lu, D. C., Liang, J. Y., Du, X. L., Wang, G. S. & Shire, T. (2019). A novel transversely isotropic strength criterion for soils based on a mobilised plane approach. *Géotechnique* **69**, No. 3, 234–250, 10.1680/jgeot.17.P.191.

Meijer, G. J., Muir Wood, D., Knappett, J. A., Bengough, A. G. & Liang, T. (2023). Root reinforcement: continuum framework for constitutive modelling. *Géotechnique* **73**, No. 7, 600–613, 10.1680/jgeot.21.00132.

Mugele, L., Niemunis, A. & Stutz, H. H. (2024). Neohypoplasticity revisited. *Numer. Analyt. Methods Geomech.* **48**, No. 1, 311–331, 10.1002/nag.3640.

Muir Wood, D., Diambra, A. & Ibraim, E. (2016). Fibres and soils: a route towards modelling of root–soil systems. *Soils Found.* **56**, No. 5, 765–778, 10.1016/j.sandf.2016.08.003.

Ng, C. W. W., Zhang, Q., Zhang, S., Lau, S. Y., Guo, H. & Li, Z. (2024). A new state-dependent constitutive model for cyclic thermo-mechanical behaviour of unsaturated vegetated soil. *Can. Geotech. J.* **61**, No. 10, 2155–2179, 10.1139/cgj-2023-0268.

Ni, X., Ye, B., Zhang, F. & Feng, X. (2021). Influence of specimen preparation on the liquefaction behaviors of sand and its mesoscopic explanation. *J. Geotech. Geoenviron. Engng* **147**, No. 2, e04020161, 10.1061/(asce)gt.1943-5606.0002456.

Norouzi, N. & Lashkari, A. (2021). An anisotropic critical state plasticity model with stress ratio-dependent fabric tensor. *Iran J. Sci. Technol. Trans. Civ. Engng* **45**, No. 4, 2577–2594, 10.1007/s40996-020-00448-z.

Rahman, S. M., Hassan, T. & Ranjithan, S. R. (2005). Automated parameter determination of advanced constitutive models. *ASME Pressure Vessels and Piping Conference*, **41871**, pp. 261–272.

Richart, F. E., Hall, J. R. Jr., & Woods, R. D. (1970). *Vibrations of soils and foundations*. Englewood Cliffs, NJ, USA: Prentice-Hall, Inc.

Seyedi Hosseininia, E. (2013). Stress–force–fabric relationship for planar granular materials. *Géotechnique* **63**, No. 10, 830–841, 10.1680/geot.12.P.055.

Shi, J., Haegeman, W., Mascini, A. & Cnudde, V. (2021). X-ray analysis on the effect of sample preparation on the microstructure of calcareous sands. *Mar. Georesour. Geotech.* **39**, No. 3, 302–311.

Stokes, A., Douglas, G. B., Fourcaud, T., Giadrossich, F., Gillies, C., Hubble, T., Kim, J. H., Loades, K. W., Mao, Z., McIvor, I. R., Mickovski, S. B., Mitchell, S., Osman, N., Phillips, C., Poesen, J., Polster, D., Preti, F., Raymond, P., Rey, F., Schwarz, M. & Walker, L. R. (2014). Ecological mitigation of hillslope instability: Ten key issues facing researchers and practitioners. *Plant Soil* **377**, No. 1–2, 1–23, 10.1007/s11104-014-2044-6.

Świtała, B. M. & Wu, W. (2018). Numerical modelling of rainfall-induced instability of vegetated slopes. *Géotechnique* **68**, No. 6, 481–491, 10.1680/jgeot.16.P.176.

Świtała, B. M., Wu, W. & Wang, S. (2019). Implementation of a coupled hydro-mechanical model for root-reinforced soils in finite element code. *Comput. Geotech.* **112**, 197–203, 10.1016/j.compgeo.2019.04.015.

Woodman, N. D., Smethurst, J. A., Roose, T., Powrie, W., Meijer, G. J., Knappett, J. A. & Dias, T. (2020). Mathematical and computational modelling of vegetated soil incorporating hydraulically-driven finite strain deformation. *Comput. Geotech.* **127**, 103754, 10.1016/j.compgeo.2020.103754.

Zhao, J. & Gao, Z. (2016). Unified anisotropic elastoplastic model for sand. *J. Engng Mech.* **142**, No. 1, 10.1061/(ASCE)EM.1943-7889.0000962.

Zhao, J. & Guo, N. (2015). The interplay between anisotropy and strain localisation in granular soils: a multiscale insight. *Géotechnique* **65**, No. 8, 642–656, 10.1680/geot.14.P.184.